

## Impacts of Mountain–Plains Solenoid on Diurnal Variations of Rainfalls along the Mei-Yu Front over the East China Plains

JIANHUA SUN

*Institute of Atmospheric Physics, Chinese Academy of Sciences, Beijing, China, and Department of Meteorology, The Pennsylvania State University, University Park, Pennsylvania*

FUQING ZHANG

*Department of Meteorology, The Pennsylvania State University, University Park, Pennsylvania*

(Manuscript received 17 February 2011, in final form 27 July 2011)

### ABSTRACT

Convection-permitting numerical experiments using the Weather Research and Forecasting (WRF) model are performed to examine the impact of a thermally driven mountain–plains solenoid (MPS) on the diurnal variations of precipitation and mesoscale convective vortices along the mei-yu front over the east China plains during 1–10 July 2007. The focus of the analyses is a 10-day simulation that used the 10-day average of the global analysis at 0000 UTC as the initial condition and the 10-day averages every 6 h as lateral boundary conditions (with diurnal variations only). Despite differences in the rainfall intensity and location, this idealized experiment successfully simulated the observed diurnal variation and eastward propagation of rainfall and mesoscale convective vortices along the mei-yu front. It was found that the upward branch of the MPS, along with the attendant nocturnal low-level jet, is primarily responsible for the midnight-to-early-morning rainfall enhancement along the mei-yu front. The MPS is induced by differential heating between the high mountain ranges in central China and the low-lying plains in east China. Diabatic heating from moist convection initiated and/or enhanced by the solenoid circulation subsequently leads to the formation of a mesoscale convective vortex that further organizes and amplifies moist convection while propagating eastward along the mei-yu front. The downward branch of the MPS, on the other hand, leads to the suppression of precipitation over the plains during the daytime. The impacts of this regional MPS on the rainfall diurnal variations are further attested to by another idealized WRF simulation that uses fixed lateral boundary conditions.

### 1. Introduction

The mei-yu front is a quasi-stationary, east–west-oriented frontal zone over East Asia during summer that often causes severe flooding along the Yangtze-Huai River Valleys (YHRV) in east China. It is characterized by weak temperature gradients and strong moisture gradients in the lower troposphere (Tao 1980; Ding 1993), which are different from typical midlatitude fronts (Shapiro and Keyser 1990). The front also has a strong cyclonic wind shear at lower levels with a well-defined low-level jet (LLJ) that transports warm moist air

northward in the lower levels (Chen 1983). It is one of the most significant weather systems for the hydrological cycle in the East Asian monsoon region.

Numerous mesoscale disturbances, including mesoscale convective systems (MCSs) or mesoscale convective vortices (MCVs), are observed to develop and propagate eastward along the frontal zone as the main makers of heavy precipitation in east China (Ding 1993; Ninomiya 2000; Zhao et al. 2004; Sun et al. 2010). For example, Zhang et al. (2004) found that most of the larger cyclonic circulations that bring heavy rainfall over YHRV along the mei-yu front are usually developed east of 115°E though there are apparent and abundant precedent smaller-scale cloud clusters upstream (west of 115°E). However, the underlying mechanisms that govern the development of these large frontal depressions and MCVs have not yet been well understood.

---

*Corresponding author address:* Dr. Fuqing Zhang, Department of Meteorology, The Pennsylvania State University, University Park, PA 16802.  
E-mail: fzhang@psu.edu

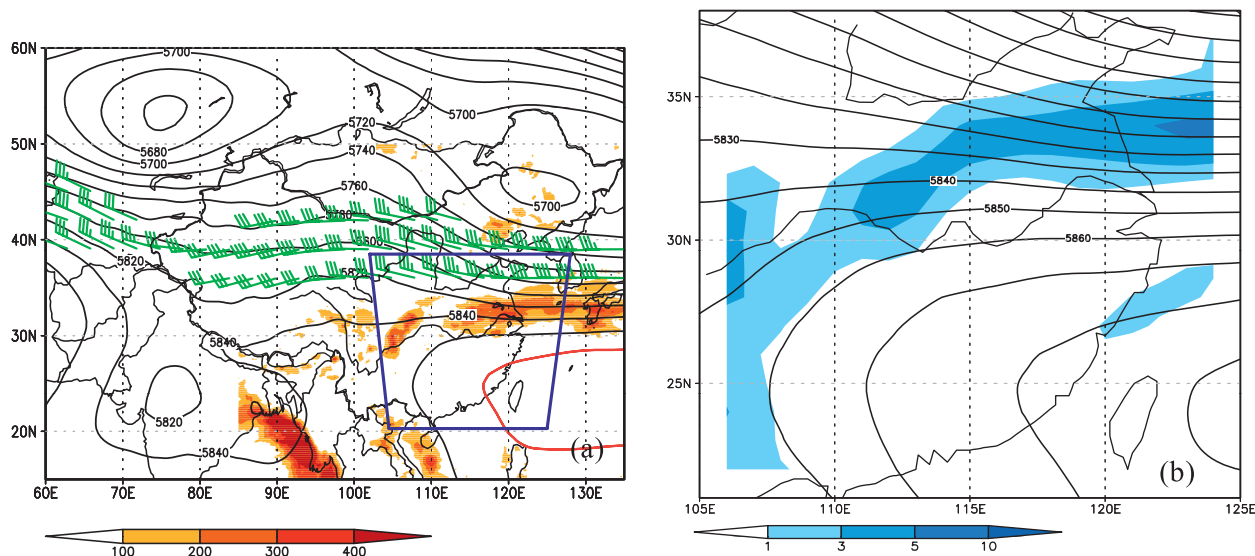


FIG. 1. (a) The average 500-hPa geopotential height (units: gpm) and 200-hPa upper-level jet greater than  $30 \text{ m s}^{-1}$  (full bar:  $10 \text{ m s}^{-1}$ ) from GFS analysis and total precipitation (CMORPH, colored, units: mm) from 0000 UTC 1 Jul to 0000 UTC 11 Jul 2007. The blue rectangle is the simulation domain. (b) The average 500-hPa geopotential height and 850-hPa relative vorticity for simulation domain (colored,  $10^{-5} \text{ s}^{-1}$ ).

With improved observing capability, recent studies have begun to document the diurnal variations of clouds and precipitation in East Asia using surface in situ measurements (e.g., Yu et al. 2007a,b) and satellite observations (Kishtawal and Krishnamurti 2001; Hirose and Nakamura 2005; Chen et al. 2009; Wang et al. 2004, 2005; Bao et al. 2011). Previous studies also showed that summertime convection in the Northern Hemisphere often develops over the high mountains in the local afternoon, which subsequently propagates eastward across the leeside plains overnight due to the forcing from diurnally varying heating (Carbone et al. 2002; Wang et al. 2005; Carbone and Tuttle 2008). For East Asia, the major terrain is the Tibetan Plateau, which is often referred to as the “first step” terrain in China, where leeside nocturnal convection near the Sichuan Basin and surrounding peripheries has been studied (Kurosaki and Kimura 2002; Yu et al. 2007a,b). The “second step” terrain in China usually refers to the high mountain ranges from the Da Hinggan Mountains over northeast China (including the Yanshan Mountains, the Taihangshan Mountains, the Loess Plateau, and the Mongolian Plateau over north China and the Qinling Mountains over central China) to the Yungui Plateau over southwest China. The “third step” terrain includes the low-lying plains and hilly regions to the east of the second-step high-mountain terrains. A recent observational study of He and Zhang (2010) showed that the second-step terrain may impact the diurnal variations of warm-season precipitation over north China through a regional-scale mountain–plains solenoid (MPS) between the mountain ranges and the

plains. It is found that the local precipitation on the eastern slope of the mountain ranges peaks in the early afternoon and the downslope propagation will result in peak precipitation around midnight and during the early morning hours over the north China plains.

The focus area of this study is over the YHRV of the east China plains to the east of second-step terrain of China during the mei-yu season. Major scientific issues are the causes of the diurnal variations of precipitation along the mei-yu front and the impacts of the second-step terrain over central China. This study period is from 1 to 10 July 2007, which features several heavy precipitation episodes with apparent diurnal variations over the east China plains. During this period, the mei-yu front extends from the foothills of the Tibetan Plateau to the east China plains with the maximum 10-day accumulated precipitation of more than 400 mm east of  $114^\circ\text{E}$  (Fig. 1a). On the synoptic scale, the western Pacific subtropical high (WPSH) at 500 hPa dominates over southeastern China with the 5860-m isohypse reaching as far west as  $110^\circ\text{E}$ . In the midlatitudes, there are two cutoff lows located at the Baikal Lake and northeast China while a synoptic ridge system controls northwest China. At 200 hPa, the midlatitude jet stream persists north of  $35^\circ\text{N}$ . Within the focus domain (the blue box in Figs. 1a and 2a), there is a strong positive relative vorticity band along the mei-yu front throughout the lower troposphere (Fig. 1b) corresponding to a shear line between the southwesterlies and northeasterlies. To the south of the shear line, there is a southwest LLJ with the wind speed maximum exceeding  $12 \text{ m s}^{-1}$  on the

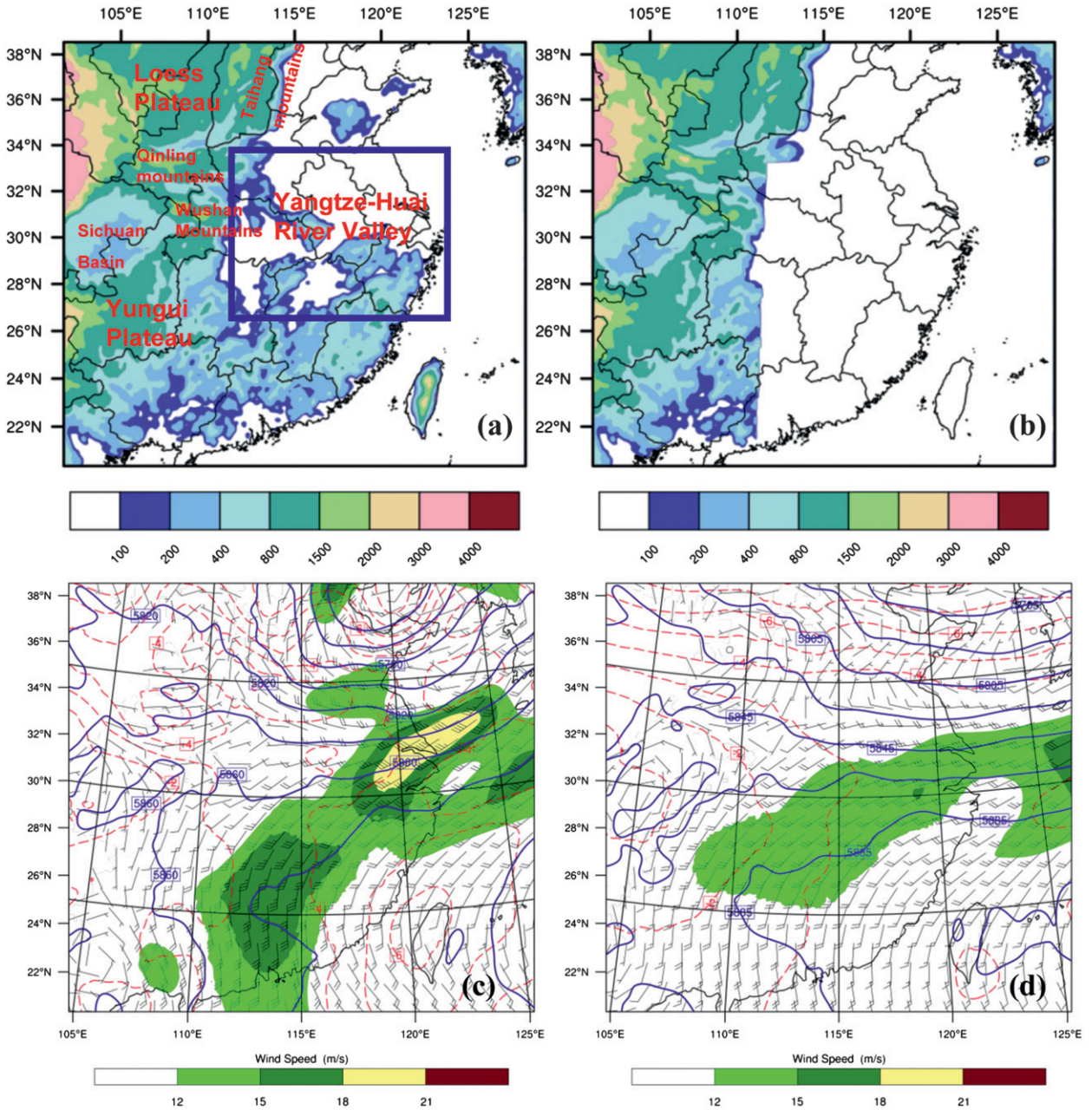


FIG. 2. The configuration of simulated domain and topography. (a) Real topography in experiments REAL, IDEAL, and DIURN, the blue rectangle shows the Yangtze-Huai River Valley. (b) The modified topography in experiment CNTL. The initial field of 500-hPa geopotential height in gpm and 500-hPa temperature in  $^{\circ}\text{C}$ , 850-hPa wind vector (full barb:  $5 \text{ m s}^{-1}$ ), and 850-hPa wind speed higher than  $12 \text{ m s}^{-1}$  (colored): (c) experiment REAL and (d) experiment IDEAL.

northwest edge of the WPSH that brings abundant warm moist air from the south (Fig. 2c). Overall, the synoptic-scale pattern is very conducive to the development of mesoscale convective systems along the mei-yu front.

The primary objective of the current study is to examine the impacts of the MPS on the diurnal variations of mesoscale convective systems and precipitation along

the mei-yu front. The experimental design is described in section 2. The overview of the simulations and comparison with the observations are presented in section 3. The MPS circulation and the diurnal precipitation variations along the mei-yu front are discussed in detail in section 4. Section 5 presents the concluding remarks of the study.

TABLE 1. A list of sensitivity experiments with different initial conditions, lateral boundary conditions, and topography.

Expt	Objectives	Initial condition	Lateral boundary condition
REAL	Real data simulation for 10 days	Initial condition at 0000 UTC 1 Jul 2007	Lateral boundary condition from real data from 0000 UTC 1 Jul to 0000 UTC 11 Jul 2007
IDEAL	Sensitivity to initial condition	Initial condition: the mean of 0000 UTC from 1 to 10 Jul 2007	As in REAL
DIURN	Sensitivity to diurnal variations and initial condition	As in IDEAL	Lateral boundary condition from mean of 0000, 0600, 1200, and 1800 UTC of 1–10 Jul 2007
CNTL	Sensitivity to topography. Removing the topography to the east of 112°E and to the south of 33.2°N over southern China	As in IDEAL	As in DIURN
FixBC	Sensitivity to lateral boundary condition	As in IDEAL	Fixed lateral boundary condition, no diurnal forcing from LBC
HIRES	Sensitivity to resolution	As in CNTL	As in CNTL

## 2. Numerical model and experimental design

The advanced research core of the Weather Research and Forecasting (WRF) model, version 3.2 (Skamarock et al. 2005) is used for this study. Only one simulation domain is used that covers part of East Asia with  $250 \times 230$  horizontal grid points and 9-km grid spacing (Fig. 2a). The western boundary of the simulation domain is purposely set at the (east) foothills of Tibetan Plateau to avoid complication and propagation of small-scale disturbances (other than the pure diurnal signals) originated from the plateau for entering the simulation domain.<sup>1</sup> There are 27 vertical levels with the top at 50 hPa. The model employs the Yonsei University (YSU) boundary layer scheme (Noh et al. 2001), the Noah land surface model (Chen and Dudhia 2001), a longwave and short-wave radiation parameterization (Dudhia 1989), a WRF Single-Moment 5-Class Microphysics Scheme (WSM5; Hong et al. 2004; Hong and Lim 2006), and a new Grell cumulus parameterization (Grell and Dévényi 2002).

The primary goal of the current study is to examine the impact of the MPS on the diurnal cycle of rainfall along the mei-yu front. The initial and lateral boundary conditions are derived from the National Oceanic and Atmospheric Administration (NOAA) Global Forecast System (GFS)  $1^\circ \times 1^\circ$  operational analyses available every 6 h. Table 1 lists the experiments and gives a brief description of each. For reference the experiments are given a four- or five-letter abbreviation. Experiment REAL is initiated at 0000 UTC 1 July 2007 with the lateral boundary conditions updated every 6 h

provided directly by the analysis from 0000 UTC 1 July to 0000 UTC 11 July 2007. Based on REAL and following Trier et al. (2010), we produced the mean final (FNL) analysis valid at 0000, 0600, 1200, and 1800 UTC averaged over the 10-day period of 1–10 July 2007. Experiment IDEAL uses the same lateral boundary conditions as REAL, but was initialized with the average of the FNL analysis at 0000 UTC for the 10-day period. Experiment DIURN uses the same 10-day-averaged initial conditions as IDEAL, but the boundary conditions are derived from the 10-day-averaged FNL analyses at 0000, 0600, 1200, and 1800 UTC, which cycle periodically in time (i.e., from 0000 to 0600 to 1200 to 1800 UTC and then back to 0000 UTC). Such lateral boundary conditions only allow the diurnal variation part of the transient processes to influence the simulation domain.

Our control experiment (CNTL) is performed the same as DIURN, but the topography to the east of 112°E and to the south of 33.2°N is removed to examine the sensitivity of the rainfall simulation to smaller mountain ranges within the east China plains and to exemplify the effect of the MPS circulation (Fig. 2b). Even with the 10-day average, the initial conditions of CNTL (as well as in IDEAL and DIURN) are mostly similar to REAL except for being apparently smoother than REAL. In consequence, the initial short-wave trough, shear line, and mesoscale vortex along the mei-yu front are much weaker in CNTL than REAL (Fig. 2c vs Fig. 2d). Experiment FixBC is the same as CNTL but uses the lateral boundary conditions as the grand 10-day average of the FNL analysis that does not vary in time. The FixBC is integrated for 30 days giving a relatively longer initial adjustment period. To examine the sensitivity of the WRF simulations to model grid spacing and cumulus parameterization, experiment HIRES is performed the same as CNTL but uses a convection-permitting

<sup>1</sup> The western boundary of the model domain so designed does intercept some complex topography. However, no significant spurious gravity waves or other numerical noises are observed to enter the domain that may adversely impact the simulation.

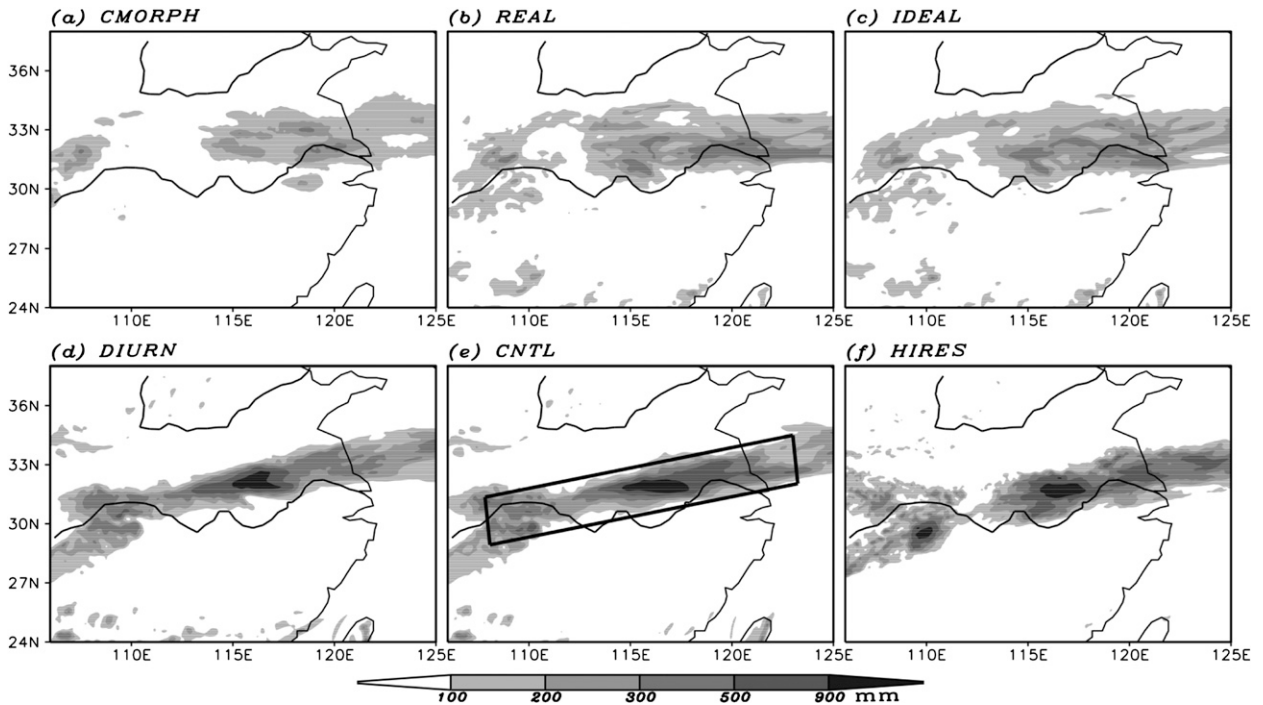


FIG. 3. Accumulated precipitation (units: mm) for the final 7 days from 0000 UTC 4 Jul to 0000 UTC 11 Jul 2007: (a) CMORPH; experiments (b) REAL, (c) IDEAL, (d) DIURN, (e) CNTL, and (f) HIRES. The black rectangle in (e) is the average rain belt area for Figs. 10 and 11.

horizontal resolution of 3 km without cumulus parameterization.

### 3. The simulated results and comparison with observations

#### a. Overview of the rainfall simulations

The accumulated precipitation of five experiments are compared with observational rainfall from the high-resolution global precipitation dataset from NOAA's Climate Prediction Center Morphing Technique (CMORPH; Joyce et al. 2004) with a spatial resolution of  $0.072 \times 77^\circ$  (Fig. 3). CMORPH has been verified with Chinese rain gauge reports from  $\sim 2000$  stations and exhibits the best performance among satellite precipitation estimates in depicting the spatial pattern and temporal variations of precipitation (Shen et al. 2010).

To lessen the sensitivity to the initial conditions, only the final 7 days of the 10-day integration are examined in this study unless otherwise specified. Figure 3 shows the comparison of the 7-day-accumulated precipitation in different simulations in comparison with the rainfall observations derived from CMORPH over the same period. Despite slightly stronger intensity and broader coverage, REAL simulates reasonably well the 7-day-accumulated total estimated by CMORPH with the

primary mei-yu frontal rainfall located between the  $29^\circ$  and  $35^\circ\text{N}$  latitude belt. There is a clear rainfall minimum along the belt between  $110^\circ$  and  $114^\circ\text{E}$  in both the observation and REAL (Figs. 3a,b). Experiment IDEAL, which is initialized with the 10-day-averaged analysis, but with the same lateral boundaries as REAL, produces similar rainfall location and intensity to REAL (and CMORPH observations) suggesting that the days 4–10 accumulated precipitation is not very sensitive to the initial conditions.

It has been widely acknowledged that propagating shortwave troughs in the midlatitude jet streams, short-term variations in the southwesterly monsoon flow, changes in the WPSH, and the eastward-propagating systems from the Tibetan Plateau are key factors in controlling the mei-yu front precipitation over East Asia (Zhang et al. 2002). To eliminate the influence of the transient component of such synoptic or subsynoptic systems, DIURN uses the 10-day-averaged diurnal tendency at the lateral boundaries (time periodic) and thus only the mean diurnal variations from outside can influence the simulation domain. Even without these transient forcings, DIURN also produces a similar rain belt along the YHRV on the east China plains, but stronger in intensity and narrower in latitudinal range compared to IDEAL and REAL (Figs. 3b–d). Further

examinations of the daily variations of the rainfall show that the difference between IDEAL and DIURN is mostly due to the north–south movement of the mei-yu front (that is induced by the aforementioned transient synoptic/subsynoptic forcings through the lateral boundaries) while the area-integrated precipitation total is similar in both experiments (not shown).

Another factor often cited as important to the mei-yu front precipitation is the presence of local topography such as the Dabieshan and Nanling Mountain ranges within or on the edge of the east China plains. Experiment CNTL sets the terrains to the east of 112°E and south of 33.2°N to 10 m, which essentially removes the smaller mountain ranges in east China and south China. Despite some small-scale temporal and spatial variations in location and intensity, the simulated 7-day-accumulated precipitation total in CNTL is similar to DIURN (Figs. 3d,e), suggesting the local topography in east and south China east of the second-step mountain ranges may have little influence on the general location and intensity of the mei-yu front precipitation belt, at least for this event. Thus, CNTL will be the primary (control) simulation that will be examined in detail in section 4.

The simulated 7-day-accumulated precipitation total to east of 114°E in the convection-permitting simulation of HIRES is also similar to CNTL (Figs. 3e,f), suggesting the mei-yu rain belt and its maximal center are not very sensitive to the cumulus scheme and horizontal grid spacing. This is different from Davis et al. (2003), who found that errors in the timing of convection, combined with propagation errors caused by cumulus parameterizations, may lead to a poor phase locking of predicted rainfall to diurnal and orographic forcing over the central United States, where a nocturnal rainfall maximum is observed.

The mean 500-hPa height and 850-hPa relative vorticity averaged over the final 7 days for different experiments are shown in Fig. 4. The simulated midlatitude trough at 500 hPa located in the northeastern domain, and the coverage and intensity of simulated WPSH<sup>2</sup> over east China in all experiments are both similar to each other and to the observational analyses (Fig. 1b). The cold air mass from the midlatitude troughs and the warm air mass associated with the location of WPSH are the most important synoptic/subsynoptic-scale factors that maintain a stable mei-yu front (Zhang et al. 2002).

<sup>2</sup> With the terrain east of 112°E and south of 33.2°N over southern China removed, the isohypse of WPSH in experiments CNTL and FixBC are smoother than the other three experiments (REAL, IDEAL, and DIURN).

On the other hand, the 850-hPa positive relative vorticity belt associated with the mei-yu front in DIURN and CNTL (Figs. 4c,d) is stronger and narrower than in REAL and IDEAL (Figs. 4a,b) as well as the observational analysis (Fig. 1b), corresponding to a stronger and narrower precipitation band in DIURN and CNTL.

### *b. The diurnal cycle of simulated precipitation*

Figure 5 shows the comparison of time–longitudinal hourly rain rate averaged from 29° to 34°N between CMORPH and the simulated final 7 days for REAL, IDEAL, and CNTL. The mei-yu season often features active periods of convection over the east China plains east of the Wushan Mountain range (~114°E) with eastward-propagating rain streaks such as in Fig. 5a. During the final 7-day simulation period, there are five such rain streaks in REAL and IDEAL as well as in the CMORPH observations (Figs. 5a–c). These rain streaks take about 30 h propagating<sup>3</sup> northeastward from 114° to 125°E with a phase speed of approximately 13 m s<sup>-1</sup>. The eastward-propagating rainfall is apparently reinforced over the plains at midnight and is intensified again near the coastline (120°E) around 0600 LST (Figs. 5a–c). With time-periodic lateral boundary conditions, the rain streaks in CNTL are similar to REAL and IDEAL but become even more regular (initiated daily) with distinct diurnal phase propagation farther to the coastal ocean (Fig. 5d). Compared to CNTL (Fig. 5d), the high-resolution convection-permitting simulation of HIRES produced similar diurnal variations though with a slightly higher rainfall intensity (Fig. 6a).

The impact of the diurnal cycle on the eastward-propagating rain streaks is further examined through sensitivity experiment FixBC that is performed the same as CNTL except that the lateral boundary conditions are a 10-day average from the same FNL analyses as the initial conditions that will not change with time (Fig. 6). Experiment FixBC simulates similar, albeit slightly less regular, diurnally propagating rain streaks to that in CNTL during days 4–10 (Fig. 5d vs Fig. 6a), which further indicates that the quasi-periodic initiation and

<sup>3</sup> In this study, the use of “propagation” and “propagating” refers to the phase speed in the ground-relative reference frame. The ground-relative propagation (phase) speed of any physical disturbances is the sum of the mean-flow speed (advection) and the intrinsic speed of the disturbance (phase or propagation speed with respect to the mean-flow or steering level winds). Given the ambiguity in pinpointing the mean flow or steering-level winds in a sheared environment, the ground-relative propagation (phase) speed, rather than the intrinsic propagation speed, can be unambiguously identified in the model simulations.

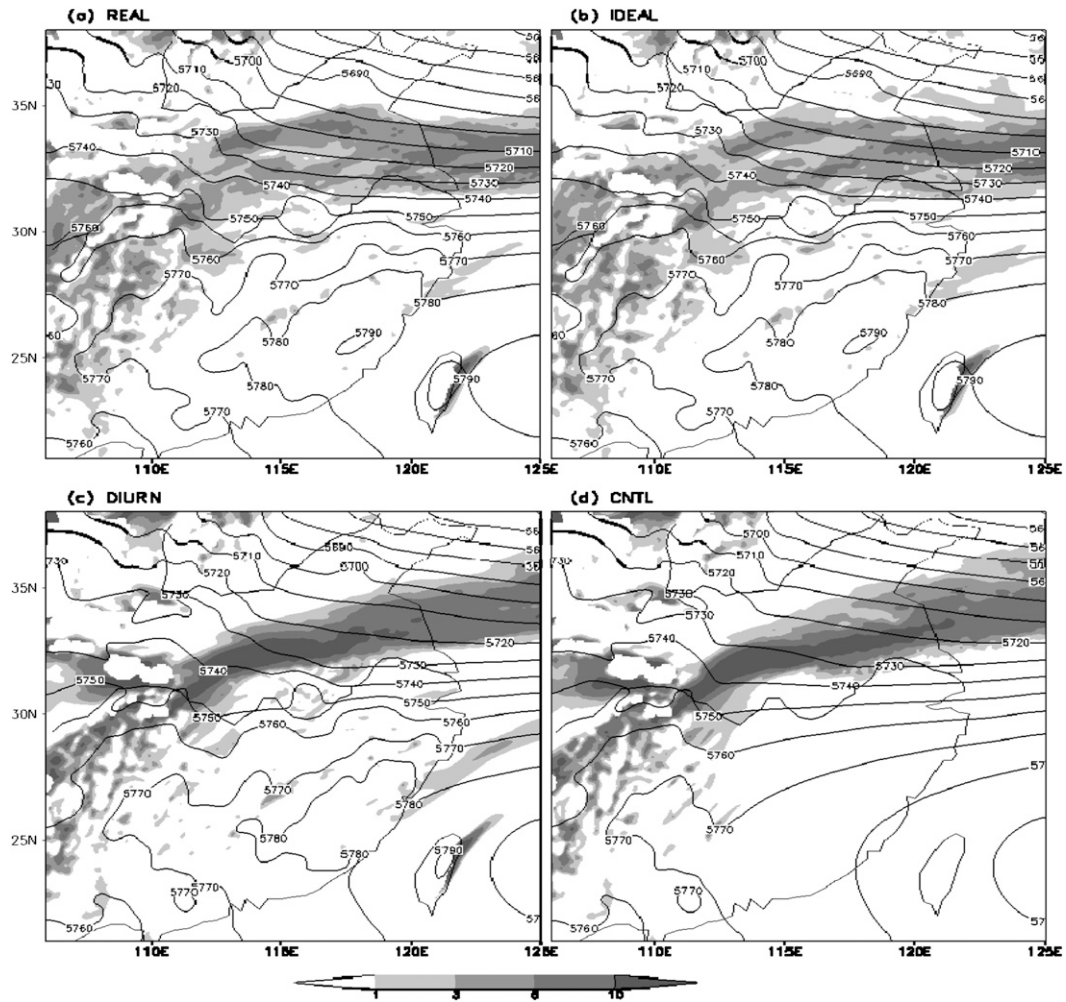


FIG. 4. The average 500-hPa geopotential height (isolines, gpm) for final 7 days and the average 850-hPa relative vorticity (shadings,  $10^{-5} \text{ s}^{-1}$ ) for final 7 days. Experiments (a) REAL, (b) IDEAL, (c) DIURN, and (d) CNTL.

propagation of the rain streaks is neither sensitive to the initial nor the lateral boundary conditions. These diurnally propagating rain streaks become more similar to CNTL during days 11–18 after further integrating FixBC for another week (Fig. 6b).

The following sections present the argument that these diurnally propagating rain streaks are strongly associated with a thermally driven MPS acting on a favorable synoptic environmental during the mei-yu season. In other words, the lower boundary forcings in the presence of large-scale topography may regulate the development of mesoscale features along the mei-yu front. On the other hand, the regularity of these diurnal-propagating rain streaks can potentially be used to at least partially extend the predictability of some precipitation systems (e.g., Pielke et al. 1991; Carbone et al. 2002).

To further elucidate the diurnal variations and propagation of the rainfall along the mei-yu front, Fig. 7

shows the Hovmöller time–longitude diagrams of the mean hourly precipitation rate averaged over the 7-day simulation for the latitude range between 29° and 34°N for REAL and CNTL. Consistent with the daily evolutions in Fig. 5, the main characteristics of the mean diurnal cycle in CNTL is broadly similar to that in REAL in terms of both timing and propagation although the intensity of nocturnal rainfall over the plains (115°–120°E) in CNTL is higher and more concentrated than in REAL (Fig. 7). As discussed earlier, the difference between REAL and CNTL is mostly due to the use of time periodic lateral boundary conditions that prevent the influence of transient subsynoptic-scale weather systems from entering the domain (except for diurnal variations). Both experiments exhibit strong diurnal variations in precipitation that differ in phase at different longitudes and thus the following discussion will focus on CNTL.

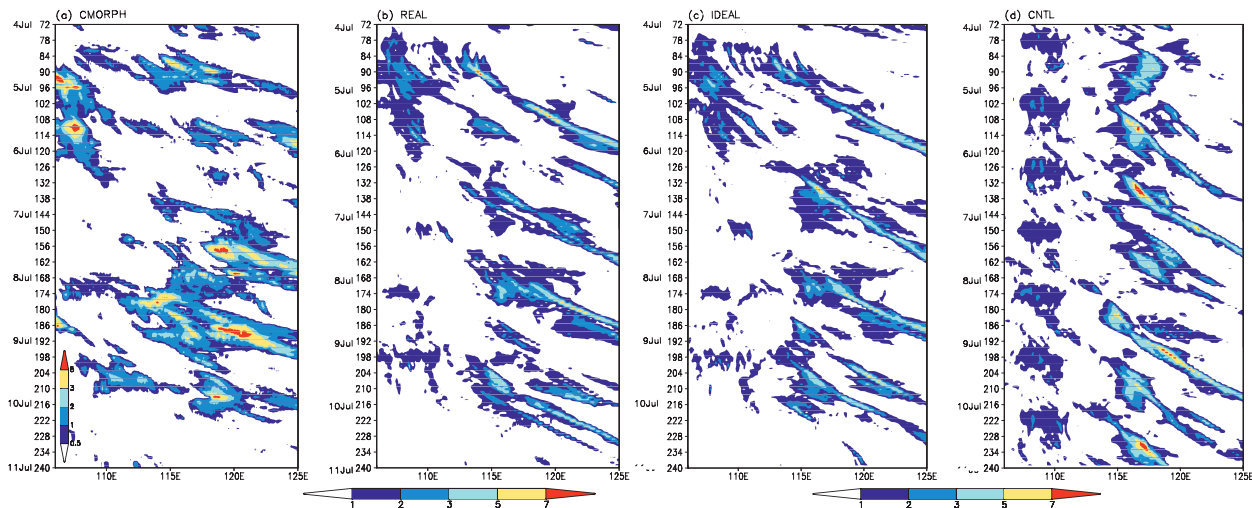


FIG. 5. The rain-rate ( $\text{mm h}^{-1}$ ) Hovmöller time–longitudinal diagram averaged from  $29^\circ$  to  $34^\circ\text{N}$  for 4–10 Jul 2007: (a) CMORPH; experiments (b) REAL, (c) IDEAL, and (d) CNTL.

Over the top of the mountain ranges near the western boundary, CNTL (as well as REAL) has the primary diurnal precipitation peak around 0600–0900 UTC [1400–1700 China Standard Time (CST)] coincident with the maximum daytime heating. The convection (C1 in Fig. 8) occurred under the southwesterly monsoon flow is possibly triggered by daytime heating. There is a secondary peak at about  $110^\circ\text{E}$  during the late evening (around 1500 UTC or 2300 CST), as marked by C2 in Fig. 8. Overall very low precipitation is simulated on the eastern slope of the mountain ranges and at the foothills ( $110^\circ$ – $114^\circ\text{E}$ ) except for a weak local maximum near noon time at about  $113^\circ\text{E}$ . Experiment CNTL has the

maximum averaged precipitation rate of  $10 \text{ mm h}^{-1}$  between  $114^\circ$  and  $118^\circ\text{E}$  starting in the late evening and ended just after sunrise (1400–0200 UTC or 2200–1000 CST) corresponding to the nocturnal precipitation maxima across the center of the east China plains. There is a clear mode of eastward phase propagation within this nocturnal precipitation peak that has an average speed of  $\sim 13 \text{ m s}^{-1}$ . Although weakened, the diurnal peak phase continues to propagate eastward reaching the eastern boundary ( $125^\circ\text{E}$ ) during the next morning ( $\sim 2100$ – $2400$  UTC or 0500–0800 CST). Near the coast and eastward, there is secondary diurnal peak that also propagates eastward at a similar speed resulting in an

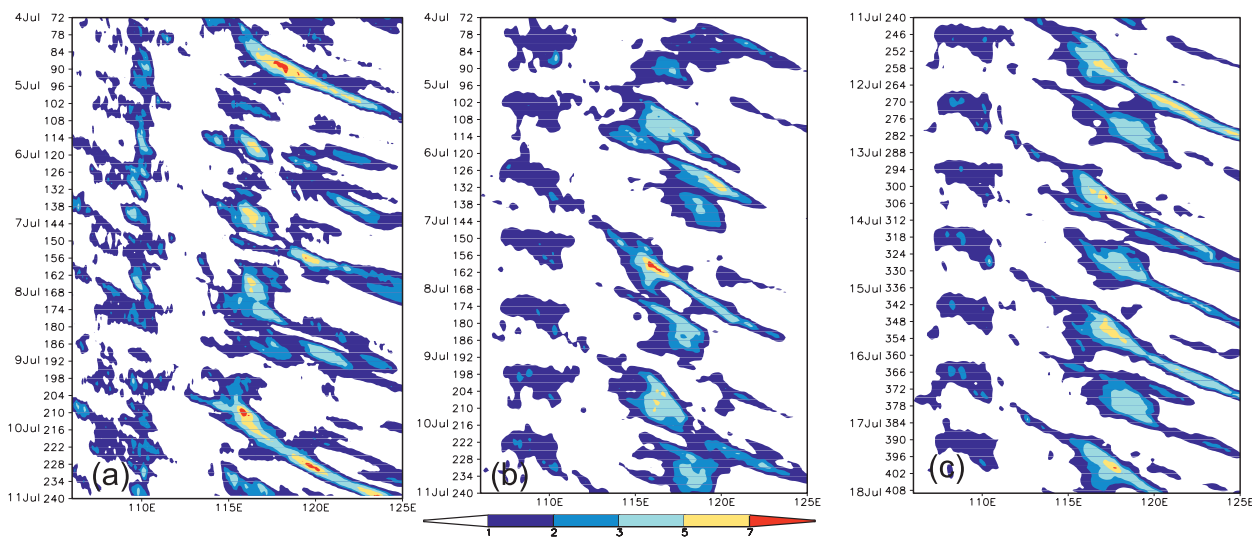


FIG. 6. The rain-rate ( $\text{mm h}^{-1}$ ) Hovmöller time–longitudinal diagram averaged from  $29^\circ$  to  $34^\circ\text{N}$  from (a) experiment HIRES for 4–10 Jul 2007, (b) experiment FixBC for 4–10 Jul 2007, and (c) experiment FixBC for 11–18 Jul 2007.

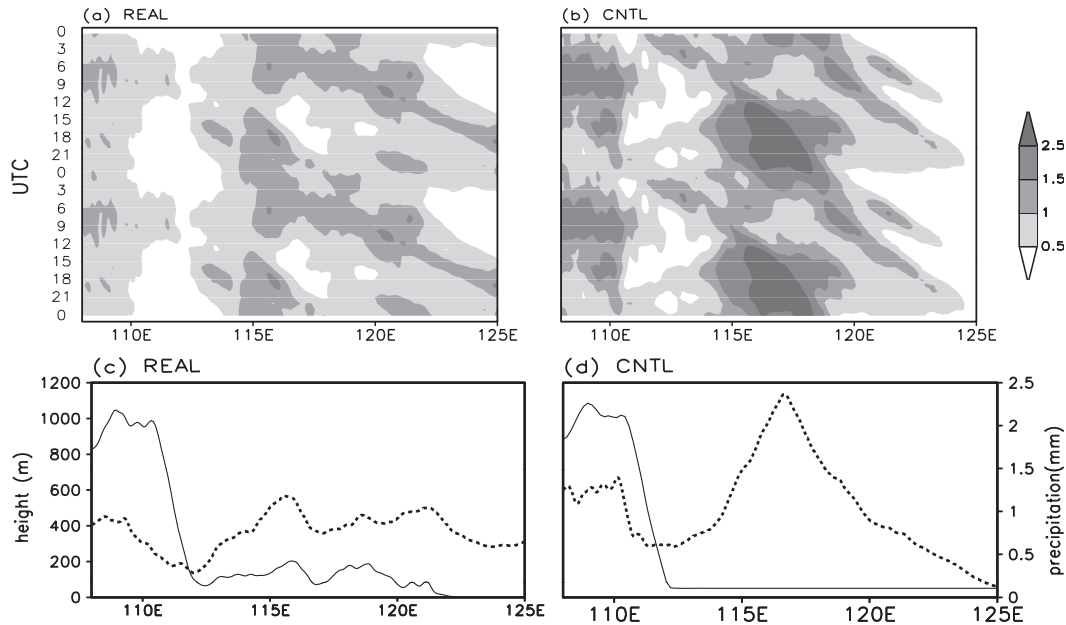


FIG. 7. The Hovmöller time-longitude diagram of the mean hourly precipitation rate averaged over the 7-day simulation for the latitude range between  $29^{\circ}$  and  $34^{\circ}\text{N}$  for experiments (a) REAL and (b) CNTL. The diurnal cycle is repeated twice for clarity across the UTC day boundary. The averaged terrain elevation of  $29^{\circ}$ – $34^{\circ}\text{N}$  latitude (black line, left coordinate) and precipitation (dashed line, right coordinate) of experiments (c) REAL and (d) CNTL.

apparent semidiurnal variation off the coast. From the daily precipitation evolution (Fig. 5d), there is also some evidence that the noontime peak at about  $113^{\circ}\text{E}$  may be the precursor of nocturnal precipitation maximum at the plains. Although inconclusive, there are some indications in both Figs. 5d and 7b that the weak precipitation maximum center over the Wushan Mountain range between  $112^{\circ}$  and  $114^{\circ}\text{E}$  may be the precursor of the precipitation maxima over the plains.

The nocturnal precipitation peak over the plains in the present study is consistent with the analysis of hourly rain gauge observations by Chen et al. (2010), which shows that many long-duration events are initiated at 1500–1900 UTC (2300–0300 CST) over this region. The rain streaks propagation from  $114^{\circ}$  to  $125^{\circ}\text{E}$  with a phase speed of  $13\text{ m s}^{-1}$  in the present event is consistent with  $13\text{ m s}^{-1}$  over north China (He and Zhang 2010) and  $14\text{ m s}^{-1}$  over the United States (Carbone et al. 2002). Carbone et al. (2002) speculated that some wavelike mechanisms, in the free troposphere and/or the planetary boundary layer, may have contributed to the rates of motion observed; the propagation speed of major episodes in their study is larger than the phase speeds of large-scale forcing or low-to-midlevel “steering” winds. As will be examined in section 3c, the eastward propagation of precipitation is closely associated with the formation and development of MCVs along the mei-yu front, whose speed is similar to the midlevel steering level winds.

### c. The diurnal cycle of simulated vortices

Figure 8 shows the map plots of mean column maximum model-simulated reflectivity and 850-hPa streamlines at different hours derived from CNTL averaged over days 4–10. Figure 9 shows the corresponding mean and anomalous vertical velocity and wind vectors and speed at 2 km AGL, but only focuses on the red box area denoted in Fig. 8. The average of all hours shown in Fig. 8a is consistent with the total precipitation distribution during the entire period (Fig. 3d) with the primary rain belt of the mei-yu front situated along the YHRV extending farther to the sea. As in Fig. 7, there are clear diurnal variations of the convective activities along the mei-yu front during this period. Overall, opposite to the diurnal heating cycle, there is clear enhancement of convective activities in the plains during the nighttime and morning hours (1400–0200 UTC or 2200–1000 CST) and a reduction in the afternoon (0600–1200 UTC or 1400–2000 CST). The timing, location, and enhancement of convection are closely associated with the development and movement of MCVs along the mei-yu front.

On the lee side of the mountain ranges east of  $110^{\circ}\text{E}$ , two mesoscale vortices exist (“V1” and “V2”) along the low-level convergence zone of the mei-yu front distinguishable in both the mean streamline field and at nearly every hour (Fig. 8a). On average, there are strong rising

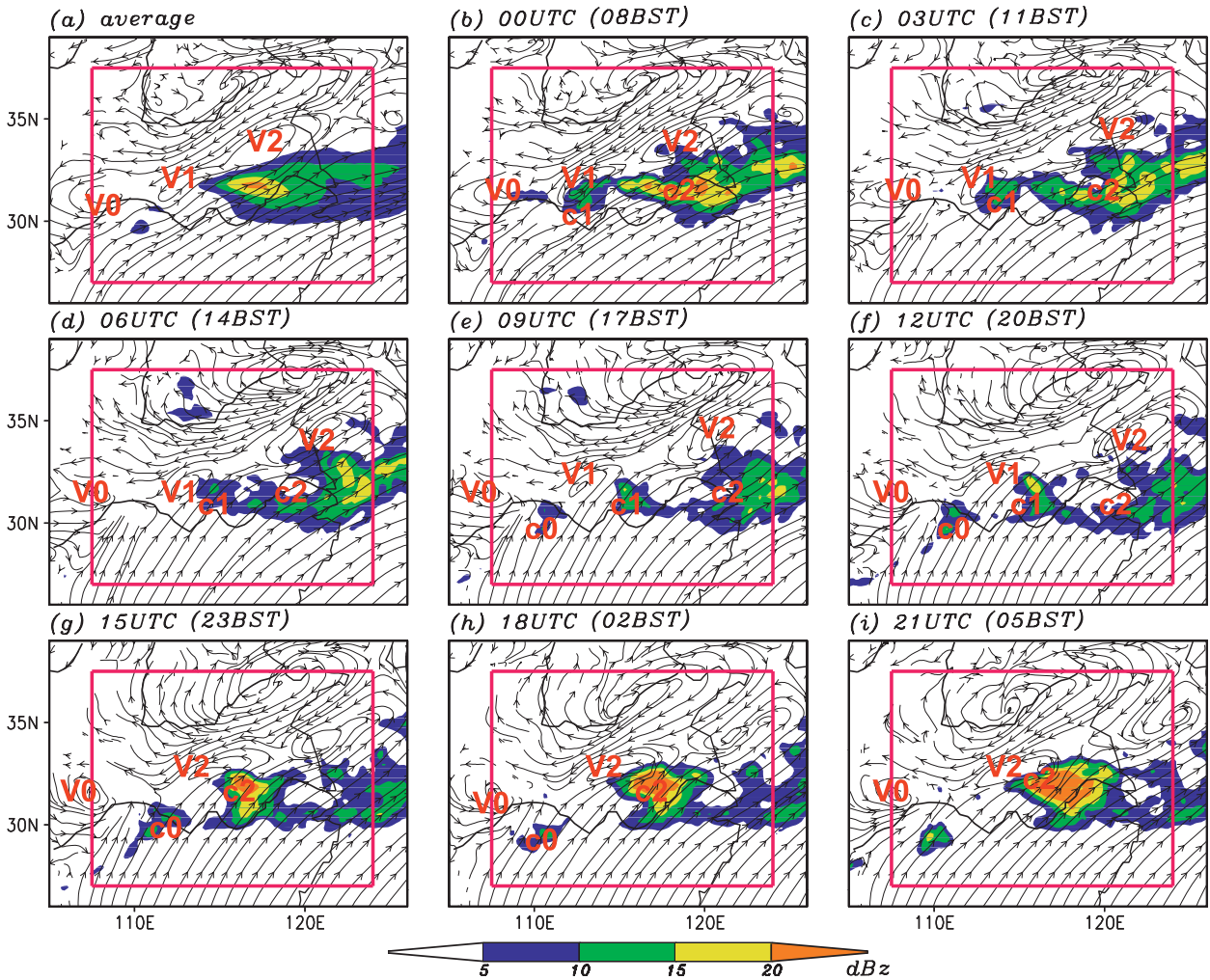


FIG. 8. The average and diurnal evolution of maximum model reflectivity in a vertical column (colored, dBZ) and 850-hPa streamline for final 7 days of experiment CNTL: (a) average, (b) 0000, (c) 0300, (d) 0600, (e) 0900, (f) 1200, (g) 1500, (h) 1800, and (i) 2100 UTC. V1 and V2 are the leeside vortex and MCV in mei-yu rain belt, respectively. The C0, C1, and C2 are the convective systems in the rain belt. The red box areas are the plot areas for Fig. 9.

motions along the mei-yu front convergence zone with strong southwesterly low-level flows to the south (Fig. 9a). The mean position of V1 is at the immediate lee of the mountain ranges, while the mean position of V2 is in the middle of the plains just north of the maximum convective activities (Fig. 8a). There is also another mesoscale vortex (“V0”) situated to the west of the mountain ranges (west of 110°E) as an eastward extension of the quasi-stationary warm-season subsynoptic-scale vortex in southwest China centered over the Sichuan Basin.

Both V1 and V2 propagate eastward with the mean steering-level flow along the low-level convergence zone of the mei-yu front, each of which has a corresponding mesoscale convective system (“C1” and “C2”) to the south and southeast. As seen in Fig. 8 and discussed in

detail below, V2 is a continuation of the previous-day V1 with the transition time marked between 1200 and 1500 UTC (2000 and 2300 CST) for easy reference. The couplet of V1 and C1 starts to form in the immediate lee of the mountain ranges around 0000 UTC (0800 CST) in the morning and subsequently travels eastward along the mei-yu front convergence zone at similar intensity until the early evening. At 1200 UTC (2000 CST), coincident with the development of a strong southwesterly LLJ (Fig. 9f), the convective activity of the couplet V1–C1 becomes considerably stronger than daytime activity (Fig. 8f). Afterward, this V1–C1 couplet develops into a much stronger MCV, the couplet of C2–V2, along with a further strengthened nocturnal LLJ at 2 km AGL with a wind speed greater than  $20 \text{ m s}^{-1}$  throughout the nighttime (Figs. 9g–i). The couplet of V2–C2 is the main

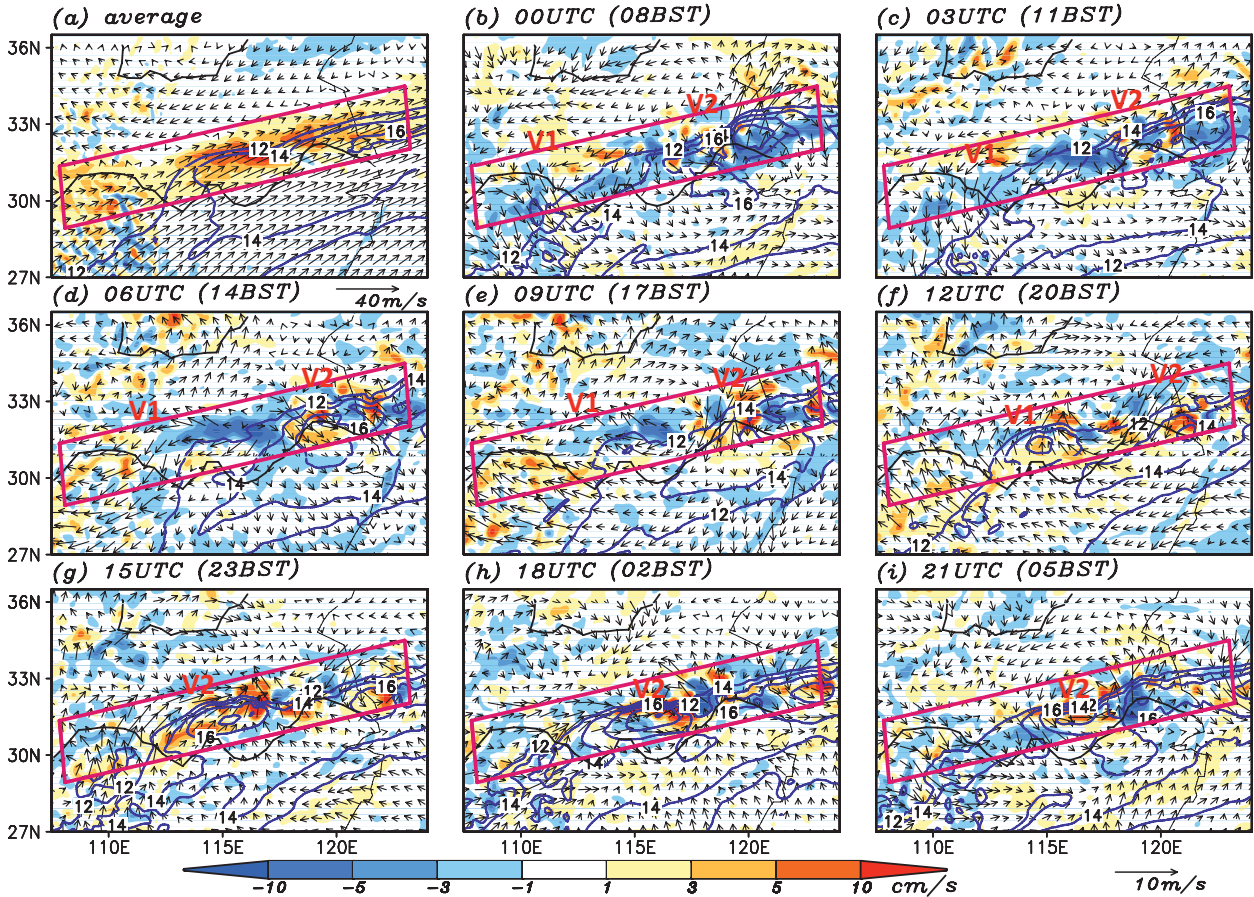


FIG. 9. (a) The average rising motion (colored,  $\text{cm s}^{-1}$ ), vector (units:  $\text{m s}^{-1}$ ), and wind speed greater than  $12 \text{ m s}^{-1}$  (blue line) at 2 km AGL of experiment CNTL. The diurnal evolution of anomalous horizontal wind (units:  $\text{m s}^{-1}$ ), vertical velocity anomalies (colored,  $\text{cm s}^{-1}$ ) and low-level jet (blue line, wind speed greater than  $12 \text{ m s}^{-1}$ ) at 2 km AGL at 3-h interval from experiment CNTL. The anomalies at each hour are relative to the 7-day average: (b) 0000, (c) 0300, (d) 0600, (e) 0900, (f) 1200, (g) 1500, (h) 1800, and (i) 2100 UTC. V1 and V2 are the leeside vortex and MCV in mei-yu rain belt, respectively. The red parallelograms are the same area as that in Fig. 3e.

rain producer during the 7-day period with most of the precipitation over the plains occurring during the nighttime and the morning hours with the maximum intensity at 1800–2100 UTC (0200–0500 CST). The center of this V2–C2 couplet begins to move out of the plains to the adjacent ocean at around 0300 UTC (1100 CST) and continues to produce rainfall over the ocean throughout the day.

The couplet of V1–C1 (and thus the subsequent V2–C2) might be related to another small mesoscale convective system (“C0”) in the southwest of the boxes ( $32^\circ\text{N}$ ,  $110^\circ\text{E}$ ; Fig. 8). The C0 starts on the east side near the top of the Wushan Mountain range around 0900 UTC (1700 CST; Fig. 8e). It briefly gains some strength and extends northeastward for the following hours until 1500 UTC (2300 CST; Fig. 8g), after which it retreats slightly southwestward before reemerging as the V1–C1 couplet at 0000 UTC (0800 CST; Fig. 8a). The C0 is

initiated on the south side of the mei-yu front convergence near the top of the mountain ranges in the mid- to late afternoon right after the peak daytime heating, which may have also benefited from enhanced convergence in the southeast side of the quasi-stationary V0 (Figs. 8f–i).

To further exemplify the relationship between the convective systems and vortices along the mei-yu rain belt based on the averaged diurnal cycle of final 7 days, a single episode of such events during 7–8 July is presented in Fig. 10. Convection activity of C0 first appears at 1500 UTC 7 July, which intensifies while moving northeastward after 2100 UTC (Figs. 10a–c) that precedes the formation of V1–C1 couplet during daytime (Figs. 10d–g). The closed circulation of the vortex V1 lasts for several hours; the eastward extension of this cyclonic circulation and the enhanced convection activity of C1 eventually leads to the formation of the

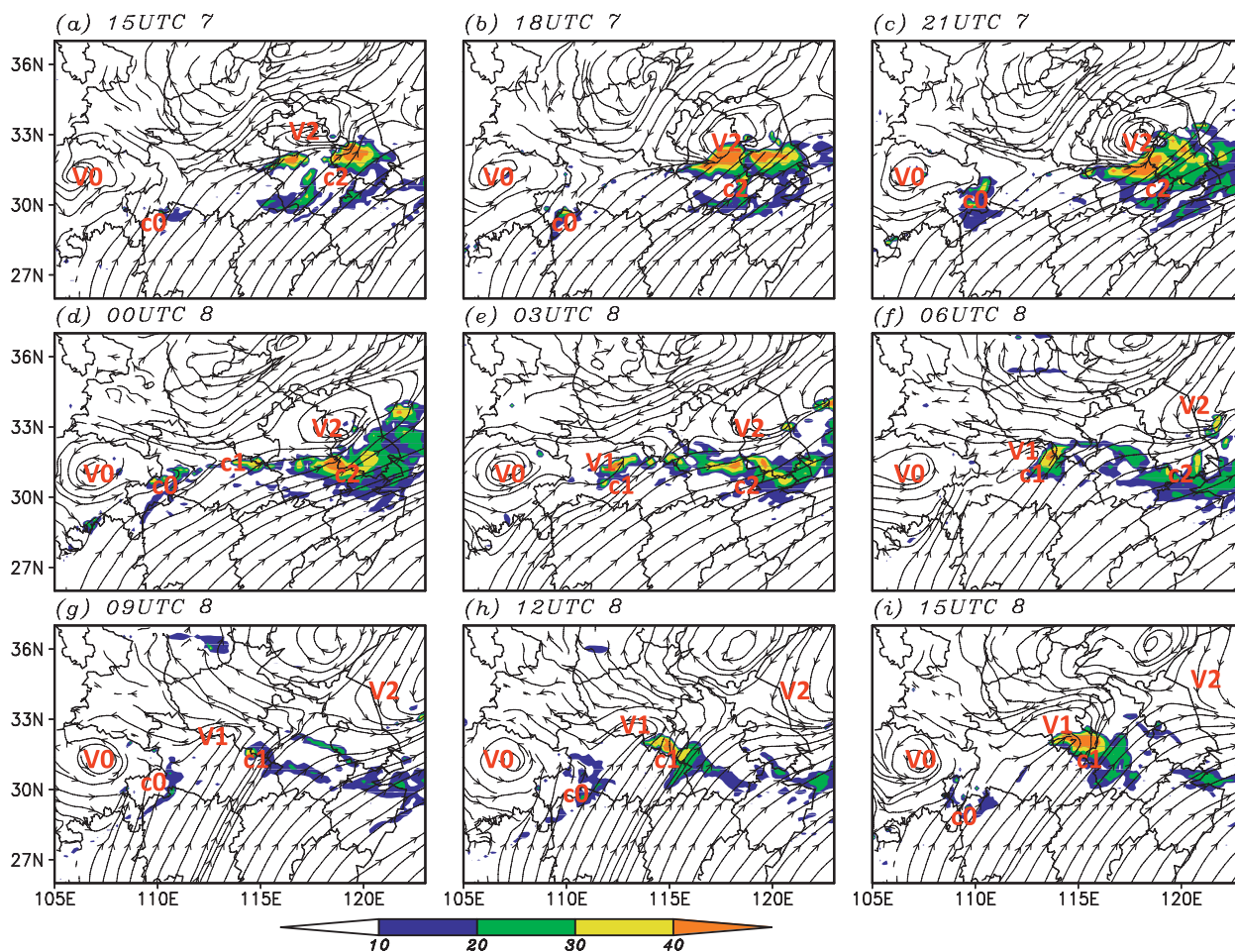


FIG. 10. The maximum model reflectivity in a vertical column (shadings, dBZ) and 850-hPa streamline of experiment CNTL from 1500 UTC 7 Jul to 1500 UTC 8 Jul 2007: (a) 1500 UTC 7 Jul, (b) 1800 UTC 7 Jul, (c) 2100 UTC 7 Jul, (d) 0000 UTC 8 Jul, (e) 0300 UTC 8 Jul, (f) 0600 UTC 8 Jul, (g) 0900 UTC 8 Jul, (h) 1200 UTC 8 Jul, and (i) 1500 UTC 8 Jul 2007. V1 and V2 are the leeside vortex and MCV in mei-yu rain belt, respectively. The C0, C1, and C2 are the convective systems in the rain belt.

MCV couplet of C1–V2 at around 1500 UTC 8 July, which becomes the major nocturnal rain producer for the next 8–9 h over the plains (Figs. 10g–i).

In summary, there are strong diurnal variations in the mesoscale vortices and convective development along the mei-yu front convergence zone over the east China plains to the lee of the Taihang–Wushan Mountain ranges. There is also apparent diurnally varying interaction between the mesoscale vortices and convection throughout the 7-day simulation. Daytime convection over the east edge of the mountain ranges, in combination with the leeside convergence may be responsible for the formation of the initial leeside vortex (V1), which is coupled with convective activity of C1 from the very beginning. The V1–C1 couplet is eventually developed into a large MCV (V2) when it moves into the plains after sunset in association with enhanced convective activities (C2) during nighttime and morning hours. The mesoscale vortices play

apparent roles in triggering and organizing moist convection along the mei-yu front, while diabatic heating from moist convection is essential in the development and strengthening of the mesoscale vortices. The nocturnal development of the mesoscale vortex V2 and convective activity C2 is further enhanced by the development of a strong nocturnal LLJ over the plains just south of the mei-yu front.

The diurnal variation of convection and precipitation along the mei-yu front in the present study is consistent with the observational study of Geng and Yamada (2007), which found an enhancement in the mei-yu front precipitation during the earlier morning. The importance of mesoscale vortices in initialization and modulation of moist convection leading to heavy localized rainfall along the mei-yu front has also long been noted in past studies (e.g., Kuo and Chen 1990; Ninomiya 2000; Zhao et al. 2004; Zhang et al. 2004; Sun et al. 2010) although

none of these studies have explicitly examined the diurnal variations of these mesoscale vortices. Existence and importance of MCVs were also noted for summertime rainfalls over North America (e.g., Smull and Houze 1985; Zhang and Fritsch 1988; Jorgensen and Smull 1993; Davis et al. 2004). The horizontal scales of these MCVs are as large as several hundred kilometers and time scales range from hours to days. An MCV is usually a result of diabatic forcing from moist convection while it can also enhance/modulate existing convection and/or initiate new secondary convection (Davis et al. 2004).

#### 4. The MPS circulation and the diurnal precipitation variations along the mei-yu front

Why do the mesoscale vortices and convection develop/strengthen at a specific location and at a particular time of the day? This section will explore the impact of a MPS induced by the differential diabatic heating between the mountain ranges and the plains on the diurnal variation and propagation of convection along the mei-yu front. Large mountain barriers have profound influences on the diurnal evolution of the atmosphere. As a result of the daytime heating forcing, convection often develops over the terrain in the local afternoon then propagates downstream to the plains. The evolution of the MPS circulations in the lee of the Rockies over North America and east of the Tibetan Plateau in East Asia, and their adjacent plains have been studied extensively in literature (e.g., Tripoli and Cotton 1986, 1989; Wolyn and McKee 1994; Zhang and Koch 2000; Koch et al. 2001; Carbone et al. 2002; Carbone and Tuttle 2008; Wang et al. 2004, 2005; Trier et al. 2006, 2010; Li and Smith 2010). However, most of these studies emphasized the impact of MPS on the warm-season precipitation under weak synoptic forcings, unlike during the mei-yu period of the current study that features strong and quasi-steady synoptic-scale frontal convergence.

##### a. The average circulation along the mei-yu rain belt

The latitudinally-averaged height–longitudinal cross sections of potential temperature, vertical velocity, and perturbation wind vectors along the mei-yu front averaged for the final 7 days of the CNTL simulation are shown in Fig. 11, while the corresponding relative humidity and horizontal wind speed are shown in Fig. 12. The latitudinal ranges used in the cross-section averages are marked by the parallelogram boxes in Figs. 3e and 9, though only the southern half of the boxes is used for the wind speed average in Fig. 12 in order to highlight the diurnal variations in the LLJ, which only

locates to the south side of the mei-yu front convergence line.

On the grand average over all times during the 7-day simulation, there are rising motions throughout the troposphere along the mei-yu front, as a reflection of persistent low-level convergence and synoptic-scale lifting. The averaged vertical motion is greater than  $8 \text{ cm s}^{-1}$  just above 1 km over the plains ( $114^{\circ}$ – $118^{\circ}\text{E}$ ; Fig. 11a) collocated with a maximum in the lower-level moisture content (Fig. 12a) as maximum convective activity and precipitation (Fig. 3e). The averaged horizontal wind speed below 3 km increases gradually from west to east (Fig. 12a). On the immediate lee of the mountain ranges, there is a slight downward motion in the lower troposphere. As the airflow passes the mountains and precipitates, the adiabatic descent leads to a potential temperature maximum and moisture minimum at the foothills of the mountain ranges (Figs. 11a and 12a), which in turn may be responsible for the rainfall minimum in this area (Fig. 3).

##### b. Diurnal evolution of the MPS circulation and its impacts

Under the mean conditions described above, there are clear diurnal variations of both the dynamic and thermodynamic variables in the cross sections of Figs. 11 and 12 that are characteristic of a regional-scale MPS. Based on the CNTL simulation, and in reference to past studies on the MPS circulation (Wolyn and McKee 1994; Zhang and Koch 2000; Huang et al. 2010), the diurnal cycle of MPS was divided into four stages: 1) the developing daytime phase (2300–0300 UTC), 2) the peak daytime phase (0400–1100 UTC), 3) the developing nighttime phase (1200–1400 UTC), and 4) the peak nighttime phase (1500–2200 UTC). As shown in Figs. 8 and 9, convection east of  $114^{\circ}\text{E}$  begins to develop during the developing nighttime phase, and the mesoscale vortex V2 dominates coupled with the strong convective activity of C2 (i.e., the MCV couplet) during the peak nighttime phase. Convection over the plains weakens during the developing daytime phase with a minimum during the peak daytime phase.

##### 1) STAGE 1: THE DEVELOPING DAYTIME PHASE OF MPS (2300–0300 UTC OR 0700–1100 CST)

The MPS circulation begins the transition from the peak nighttime phase to the developing daytime phase just before 0000 UTC (0800 CST), shortly after sunrise, and prior to significant daytime heating (Figs. 9b, 11b, and 12b). Above 2 km AGL, there are anomalous westerly flows with varying strength from the top of the mountains all the way to the coastal areas (Fig. 11b). On the foothills ahead of the downslope perturbation wind maximum exists a weak leeside convergence zone

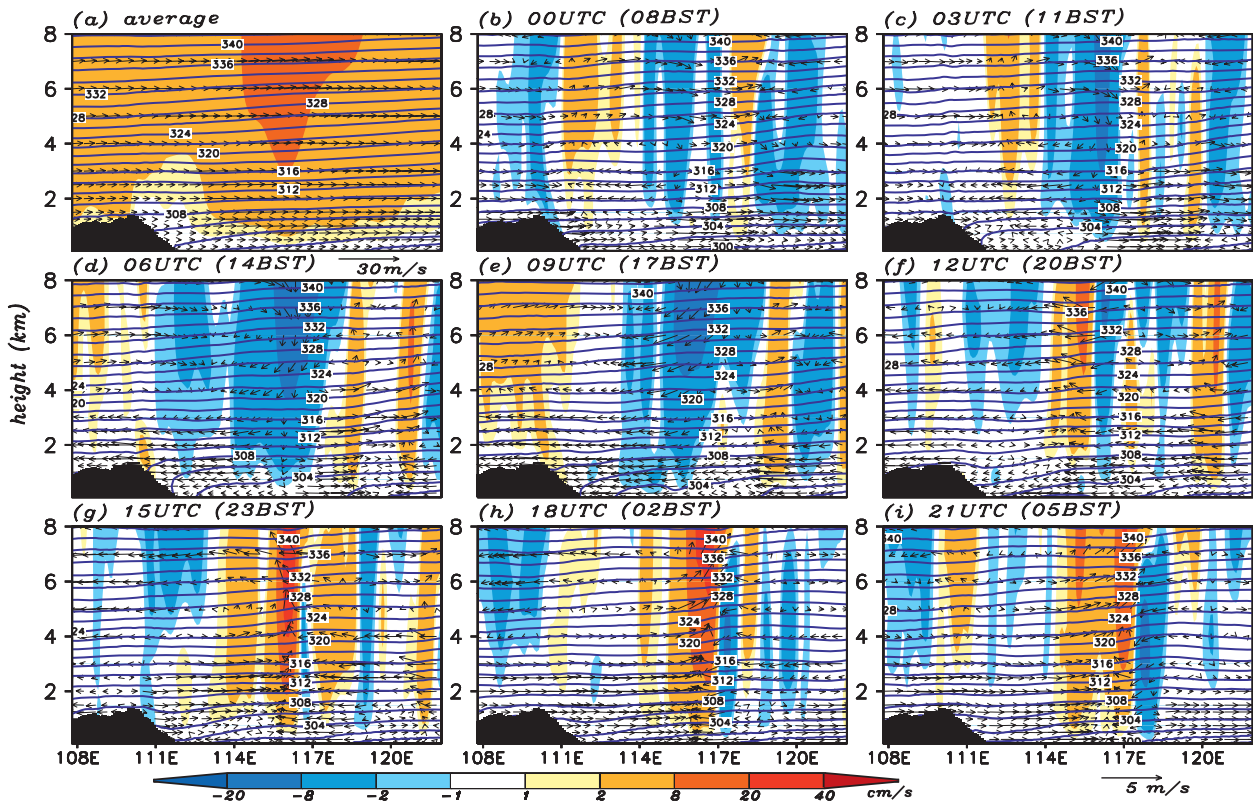


FIG. 11. (a) The height-longitudinal cross section of daily mean potential temperature (solid line, K), vertical velocity (colored,  $\text{cm s}^{-1}$ ), and vector of zonal wind and vertical velocity. (b)–(i) The diurnal evolution of potential temperature (solid line, K), perturbation vertical velocity (colored,  $\text{cm s}^{-1}$ ), and vector of anomalous zonal wind and anomalous vertical velocity ( $\times 10$ ) of experiment CNTL at a 3-h interval. The black shadings are topography.

( $112^{\circ}$ – $114^{\circ}\text{E}$ ) where there are also weak upward motions in the low- to midtroposphere. The descending motion prevails over most of the rest of the cross section except for another narrow zone of weak upward motion on the coastal land. Over the plains, the gradual increase of low-level westerly wind speed from the foothills to the plains corresponds to weak divergence (along with downward motions; Fig. 12b). In the meantime, the decaying MCV couplet (V2–C2; Fig. 8b) induces the horizontal wind speed maximum and the upward motion near the coastal areas, which persists throughout the day as the couplet slowly moves off the coast (Figs. 8c–f).

At 0300 UTC (1100 CST), differentially stronger surface heating on the terrain slopes results in the near-surface flow reversal to easterlies (Fig. 11c), the demise of downward motion over the mountain top and eastern slope, and an upward bulging of the near-surface isentropes (due to adiabatic cooling by weak ascent). The low-level flow reversal also leads to stronger divergence and downward motion anomalies over the plains (as the downward branch of the developing daytime MPS) resulting in reduced convective activities (Figs. 8b,c and

9b,c) in this region despite very strong low-level moisture content (Figs. 12b,c). In the meantime, the developing leeside convergence, and the upward branch of the developing MPS on the foothills of the mountains, albeit weak, may be essential in the formation of the MCV couplet (V1–C1).

## 2) STAGE 2: THE PEAK DAYTIME PHASE OF MPS (0400–1100 UTC OR 1200–1900 CST)

The MPS circulation transitions to the peak daytime phase at around noontime and lasts throughout the afternoon hours with anomalous rising motions spanning from the terrain slope to the top of the mountain ranges and with anomalous sinking motions across the plains (Figs. 11d,e and 12d,e). This compensating branch of the MPS over the plains induces subsidence, divergence, and midtropospheric drying resulting in much reduced convective activities over the plains in the afternoon (Figs. 8d,e and 9d,e). In the meantime, the LLJ over the plains is further weakened with the core moving out to sea along with the decaying V2–C2 couplet (Figs. 9d,e and

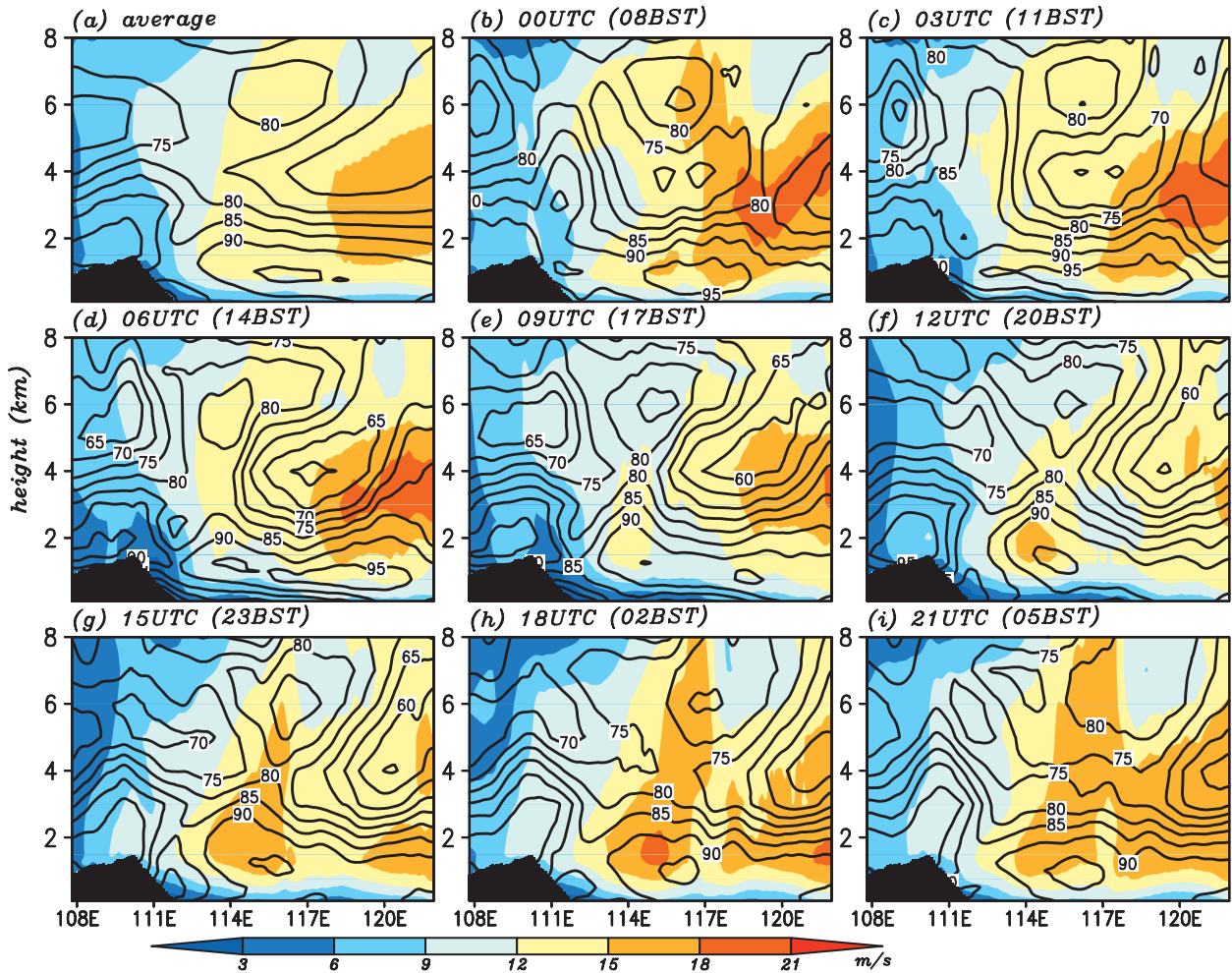


FIG. 12. The height-longitudinal cross section of relative humidity (black solid line, %) and wind speed (colored,  $m\ s^{-1}$ ) from experiment CNTL: (a) daily mean and (b)–(i) diurnal cycle at a 3-h interval. The black shadings are topography.

12d,e). Nevertheless, the V1–C1, despite considerably weakened, survives the adverse effect by the downward branch of the MPS over the plains (Figs. 9d,e).

3) STAGE 3: THE DEVELOPING NIGHTTIME PHASE OF MPS (1200–1400 UTC OR 1900–2200 CST)

The MPS circulation transitions into the developing nighttime phase at about 1200 UTC. Most notably, with the loss of solar heating on the eastern slope of the mountains, the upslope easterly anomalies (due to the differential daytime heating) begin to weaken and then reverse to westerlies from the foothills and to the terrain slope (Fig. 11f). The wind reversal east of the foothills leads to low-level horizontal convergence, which collocates with the remnant C1–V1 couplet on the plains (centered around 115°E), and revives the convection associated with V1 (Fig. 11f). The changes in the relative

humidity distribution, on the other hand, are rather small from the peak daytime phase (Figs. 12d–f).

4) STAGE 4: THE PEAK NIGHTTIME PHASE OF MPS (1500–2200 UTC OR 2300–0600 CST)

During the peak nighttime phase, the MPS circulation is characterized by prevailing upward motions all across the plains and prevailing downward motions on the terrains to the west (Figs. 9g–i and 11g–i). In the meantime, the reinvigorated C1–V1 couplet gradually develops into a long-lived MCV, relabeled as the C2–V2 couplet, that will persist throughout the next day as it moves from the plains to the coast bringing heavy rainfalls all along the mei-yu front. Heavy precipitation also induces strong downdrafts within the C2–V2 couplet over the plains in the late hours of this stage (Fig. 11i).

### c. Diurnal variations of LLJ and the mei-yu front

Besides the MPS circulation, diurnal variation of the LLJ and the mei-yu front itself may also have an impact on the development of mesoscale vortices and convection along the mei-yu rain belt. Past studies have noted that the peak rainfall along the mei-yu front usually occurred in the early morning hours before sunrise (Hirose and Nakamura 2005; Geng and Yamada 2007). Figure 13 shows the vertical cross section across the mei-yu front averaged from 114° to 120°E (the main rain belt; Figs. 8a and 9a). On the daily average, there are broad rising motions between 31° and 33°N along the mei-yu front convergence zone with the southwesterly LLJ greater than 15 m s<sup>-1</sup> below 2 km AGL (Fig. 13a). However, there are strong diurnal variations of the cross-frontal circulation and the LLJ. For example, at 0600 UTC (1400 CST) during the peak daytime phase, there are anomalous downward motions and anomalous low-level divergences at the core latitude of the mei-yu front (~32°N) corresponding to the daytime minimum convective activity along the mei-yu front (Figs. 8d and 13b). On the other hand, at 1800 UTC (0200 CST) during the peak nighttime phase, there are strong anomalous rising motions and a strong anomalous low-level convergence corresponding to vigorous development of the C2–V2 couplet and nocturnal precipitation maximum along the mei-yu front (Figs. 8h and 13c). Correspondingly, the LLJ to the south of the mei-yu front is also much stronger in the boundary layer during the nocturnal phase (Fig. 13c) than during the daytime (Fig. 13b). This is most evident at around 115°E where the LLJ varies from less than 12 m s<sup>-1</sup> at 0600 UTC to over 18 m s<sup>-1</sup> at 1800 UTC (Fig. 12) corresponding to a focused nocturnal ascent near this longitude (Fig. 11). Besides the influence of the MPS, strong diurnal variations of the LLJ are apparently another strong contributor to the rainfall variations along the mei-yu front. The importance of the nocturnal LLJ to the diurnal cycle of rainfall has long been recognized over the Great Plains of the United States (Means 1954; Bonner 1968; Frisch et al. 1992; Carbone and Tuttle 2008; Blackadar 1957; Holton 1967) as well as over east China (Miller and Fritsch 1991). The diurnal variations of the LLJ may be due to two processes: a sudden reduction in eddy viscosity due to the nocturnal stabilization of the boundary layer (Blackadar 1957) and the diurnal oscillation of the pressure gradient force due to the heating/cooling of sloped terrains (Holton 1967).

### d. A schematic model on the influence of MPS

Based on the analyses of the diurnal variations of the MPS, LLJ, and the mei-yu front in previous subsections, a schematic model is proposed to summarize the key

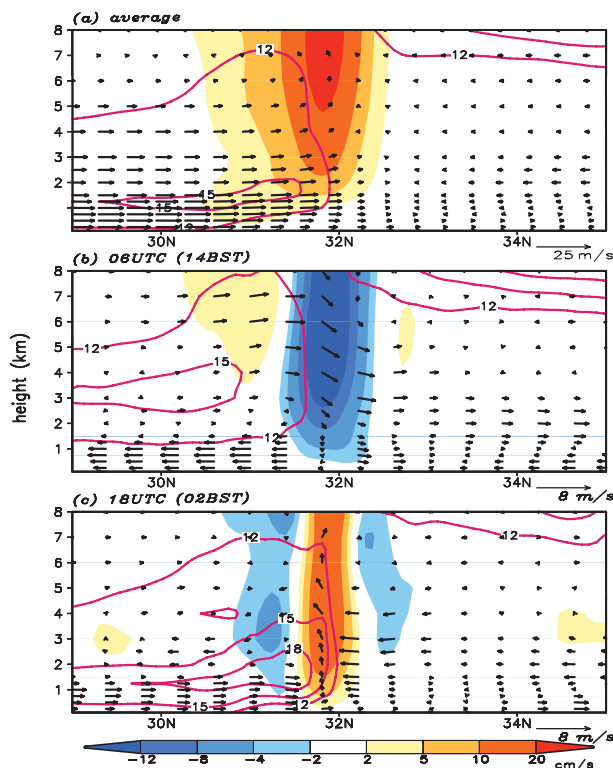


FIG. 13. (a) The height–latitude cross section of vector of zonal wind and vertical velocity (colored, cm s<sup>-1</sup>) and wind speed (pink line, greater than 12 m s<sup>-1</sup>) averaged from 114° to 120°N. The height–latitude cross section of vector of anomalous zonal wind and anomalous vertical velocity (colored, cm s<sup>-1</sup>) and wind speed (pink line, greater than 12 m s<sup>-1</sup>) averaged from 114° to 120°N from experiment CNTL at (b) 0600 and (c) 1800 UTC.

processes that are responsible for the precipitation diurnal cycles along the mei-yu front over the east China plains (Fig. 14). During the mei-yu season, under the influence of both the WPSH and the midlatitude westerlies, the west-southwest–east-northeast-oriented quasi-stationary mei-yu front extends from southwest China to the eastern seaboard with two vortices (V1 and V2) dominating convections east of 110°E positioned at the immediate lee of second-step terrains and in the middle of the plains, respectively. Besides the strong moisture gradient, the front is also a strong convergent sheared zone featuring southwesterly winds to the south and northeasterly winds to the north (Fig. 14a).

In the mid- to late morning hours, a moderate mesoscale convective system is first developed within the upward branch of the developing daytime MPS circulation at the foothills of the mountain ranges (second-step terrain; Fig. 14b). Convection, along with the leeside convergence zone (and leeside vortex), leads to the formation of a MCV (C1–V1 couplet) during the daytime, which weakens as it moves eastward toward the middle of the east China plains

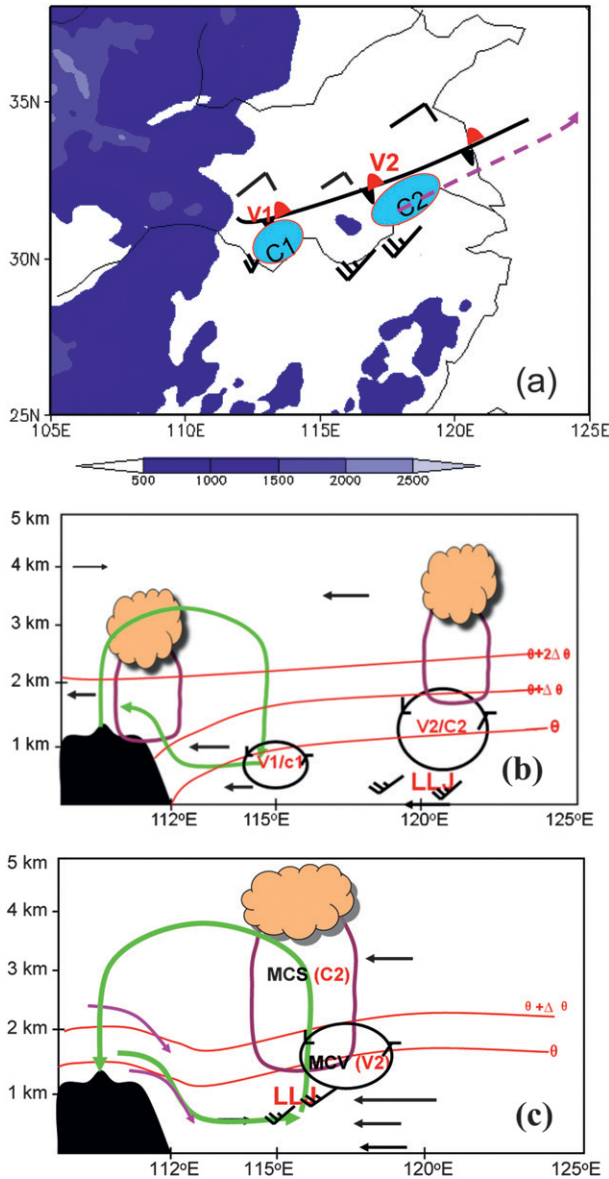


FIG. 14. The conceptual model of the nighttime rain-rate peak in the mei-yu front. (a) The horizontal distribution of MCS and lee-side vortex and MCV in the mei-yu front. The pink dashed line is the moving track of MCV. Blue shadings: topography higher than 500 m. The vertical cross section distribution of all systems associating with the (b) daytime rain-rate peak and (c) nighttime rain-rate peak. Red line: potential temperature; solid arrows: anomalous wind; green line: MPS circulation; and pink line: the rising and sinking motions. V1–C1 and V2–C2 are the MCVs and coupled convections.

dominated by the downward branch of the MPS (corresponding to daytime precipitation minimum in this area) while the remnant previous-day C2–V2 couplet gradually moves into the ocean (Fig. 14b). As the MPS transitions to the nocturnal phase, the upward branch of the MPS begins to dominate over the plains; this, along with the coincident

strengthening low-level southwesterly jet, reinvigorates convection associated with the C1–V1 couplet, which eventually leads to the development of a large MCS (i.e., the C2–V2 couplet) and the nocturnal rainfall maximum over a broad area of the east China plains along the mei-yu front (Fig. 14c).

It is worth noting that Tripoli and Cotton (1989) also proposed a conceptual model of the orogenic MCS structure and development over the Rockies, which is under weak synoptic forcings. The MPS circulation of the current study due to the altitude contrast between the second-step mountain ranges and the east China plains is further influenced by the background vorticity, abundant moisture, and strong synoptic forcing provided by the quasi-steady mei-yu front, which are much more favorable for the MCS/MCV development.

5. Conclusions

This study examines the impact of a mountain–plains solenoid (MPS) on the diurnal variations of precipitation and mesoscale convective vortices (MCVs) along the mei-yu front through convection-permitting Weather Research and Forecasting (WRF) simulations. The period of interest is 1–10 July 2007 and features several episodes of eastward-propagating heavy precipitation over the east China plains that are originated from the high mountain ranges of the “second-step” China terrains with apparent diurnal variations. Despite differences in rainfall intensity and location, the WRF simulations with both observed (real) and averaged (idealized) initial and boundary conditions and/or simplified terrains over east China successfully simulated the observed diurnal variation and eastward propagation of rainfalls and MCVs along the mei-yu front.

Detailed analyses were performed on experiment DIURN that used the 10-day average of the global analysis at 0000 UTC as the initial conditions and the 10-day averages every 6 h as lateral boundary conditions (with diurnal variations only). It was found that the upward branch of the MPS, along with the attendant nocturnal low-level jet (LLJ), is primarily responsible for the midnight to early-morning rainfall enhancement along the mei-yu front. The MPS is induced by differential heating between the high mountain ranges in central China and the low-lying plains in east China. Diabatic heating from moist convection initiated by the MPS subsequently leads to the formation of an MCV that further organizes and amplifies moist convection while propagating eastward along the mei-yu front. The downward branch of the MPS, on the other hand, leads to the suppression of precipitation over the plains during the daytime. The eastward propagation speed of the precipitation maximum and the MCVs is approximately  $13 \text{ m s}^{-1}$ ,

which is likely determined by the midtropospheric steering level flow and the intrinsic speed of the disturbance as shown in He and Zhang (2010) and Bao et al. (2011).

The impacts of this regional MPS on the rainfall diurnal variations are further attested by another idealized WRF simulation (FixBC) that is performed similar to DIURN but with fixed lateral boundary conditions. On the other hand, given the similarity between IDEAL and DIURN, it was concluded that the small topography over east and south China east of the second-step terrain has minimal impacts on the diurnal variations of precipitation over the east China plains. The simulated rain-rate streaks from FixBC further reveal that the regular diurnal cycle dominates the rainfall pattern after 5 days (Fig. 6), which is only 2 days later than CNTL. The similar periodic diurnal cycle in FixBC from simulated 5–30 days further suggested that the nocturnal convection peak is enhanced by local forcing, which also indicates that topography may control the development of mesoscale features and thus extend their predictability (Pielke et al. 1991).

The relationship between nocturnal low-level jets (NLLJs) of the Great Plains of North America and rainfall have been studied by Tuttle and Davis (2006) and Carbone and Tuttle (2008). The basic findings are that enhanced precipitation generally occurred near the exit region of the LLJ if there is weak baroclinity. The east China NLLJ has been associated with nocturnal mesoscale convective activities by Miller and Fritsch (1991). However, although the east China NLLJ lies to the east of mountain range like NLLJs of the Great Plains, large-scale forcing plays a more important role in modulating the China NLLJ than it does for the NLLJs of the Great Plains (Monaghan et al. 2010). In the current study, despite clear association of the diurnal variations of the precipitation over the plains with an attendant LLJ, there exists complex relationship between LLJ and convection/vortex in the mei-yu front. Future studies should explore the mechanisms that are responsible for the LLJ diurnal variations and its accurate impacts on diurnal cycle of precipitation. The current study also does not explore the mechanisms that are responsible for the initiation, maintenance, and intensification of the long-lived diurnally varying MCVs. It also remains to be further explored in future studies how general are the rainfall diurnal variations observed in this single case study.

*Acknowledgments.* This study is jointly sponsored by the National Natural Science Foundation of China under Grants 40875021 and 40930951, and by the U.S. National Science Foundation under Grants 0904635 and 1114849.

## REFERENCES

- Bao, X., F. Zhang, and J. Sun, 2011: Diurnal variations of warm-season precipitation east of the Tibetan Plateau over China. *Mon. Wea. Rev.*, **139**, 2790–2810.
- Blackadar, A. K., 1957: Boundary layer wind maxima and their significance for the growth of nocturnal inversions. *Bull. Amer. Meteor. Soc.*, **38**, 283–290.
- Bonner, W. D., 1968: Climatology of the low-level jet. *Mon. Wea. Rev.*, **96**, 833–850.
- Carbone, R. E., and J. D. Tuttle, 2008: Rainfall occurrence in the United States warm season: The diurnal cycle. *J. Climate*, **21**, 4132–4136.
- , —, D. Ahijevych, and S. B. Trier, 2002: Inferences of predictability associated with warm season precipitation episodes. *J. Atmos. Sci.*, **59**, 2033–2056.
- Chen, F., and J. Dudhia, 2001: Coupling an advanced land surface–hydrology model with the Penn State–NCAR MM5 modeling system. Part I: Model implementation and sensitivity. *Mon. Wea. Rev.*, **129**, 569–585.
- Chen, G., W. Sha, and T. Iwasaki, 2009: Diurnal variation of precipitation over southeastern China: Spatial distribution and its seasonality. *J. Geophys. Res.*, **114**, D13103, doi:10.1029/2008JD011103.
- Chen, G. T.-J., 1983: Observational aspects of Mei-yu phenomena in subtropical China. *J. Meteor. Soc. Japan*, **61**, 306–312.
- Chen, H., R. Yu, J. Li, W. Yuan, and T. Zhou, 2010: Why nocturnal long-duration rainfall presents an eastward-delayed diurnal phase of rainfall down the Yangtze River Valley. *J. Climate*, **23**, 905–917.
- Davis, C. A., K. W. Manning, R. E. Carbone, S. B. Trier, and J. D. Tuttle, 2003: Coherence of warm-season continental rainfall in numerical weather prediction models. *Mon. Wea. Rev.*, **131**, 2667–2679.
- , and Coauthors, 2004: The Bow Echo and MCV Experiment: Observations and opportunities. *Bull. Amer. Meteor. Soc.*, **85**, 1075–1093.
- Ding, Y. H., 1993: *Study on the Lasting Heavy Rainfalls over the Yangtze-Huaihe River Basin in 1991* (in Chinese). Chinese Meteorological Press, 255 pp.
- Dudhia, J., 1989: Numerical study of convection observed during the winter monsoon experiment using a mesoscale two dimensional model. *J. Atmos. Sci.*, **46**, 3077–3107.
- Frisch, A. S., B. W. Orr, and B. E. Martner, 1992: Doppler radar observations of the development of a boundary-layer nocturnal jet. *Mon. Wea. Rev.*, **120**, 3–16.
- Geng, B., and H. Yamada, 2007: Diurnal variations of the Meiyu/Baiu rain belt. *SOLA*, **3**, 61–64.
- Grell, G. A., and D. Dévényi, 2002: A generalized approach to parameterizing convection combining ensemble and data assimilation techniques. *Geophys. Res. Lett.*, **29**, 1693, doi:10.1029/2002GL015311.
- He, H., and F. Zhang, 2010: Diurnal variations of warm-season precipitation over North China. *Mon. Wea. Rev.*, **138**, 1017–1025.
- Hirose, M., and K. Nakamura, 2005: Spatial and diurnal variation of precipitation systems over Asia observed by the TRMM Precipitation Radar. *J. Geophys. Res.*, **110**, D05106, doi:10.1029/2004JD004815.
- Holton, J. R., 1967: The diurnal boundary layer wind oscillation above sloping terrain. *Tellus*, **19**, 199–205.
- Hong, S.-Y., and J.-O. J. Lim, 2006: The WRF Single-Moment 6-Class Microphysics Scheme (WSM6). *J. Korean Meteor. Soc.*, **42**, 129–151.

- , J. Dudhia, and S.-H. Chen, 2004: A revised approach to ice microphysical processes for the bulk parameterization of clouds and precipitation. *Mon. Wea. Rev.*, **132**, 103–120.
- Huang, H.-L., C.-C. Wang, G. T.-J. Chen, and R. E. Carbone, 2010: The role of diurnal solenoidal circulation on propagating rainfall episodes near the eastern Tibetan Plateau. *Mon. Wea. Rev.*, **138**, 2975–2989.
- Jorgensen, D. P., and B. F. Smull, 1993: Mesovortex circulations seen by airborne Doppler radar within a bow-echo mesoscale convective system. *Bull. Amer. Meteor. Soc.*, **74**, 2146–2157.
- Joyce, R. J., J. E. Janowiak, P. A. Arkin, and P. Xie, 2004: CMORPH: A method that produces global precipitation estimates from passive microwave and infrared data at high spatial and temporal resolution. *J. Hydrometeorol.*, **5**, 487–503.
- Kishtawal, C. M., and T. N. Krishnamurti, 2001: Diurnal variation of summer rainfall over Taiwan and its detection using TRMM observations. *J. Appl. Meteor.*, **40**, 331–344.
- Koch, S. E., F. Zhang, M. L. Kaplan, Y.-L. Lin, R. Weglarz, and C. M. Trexler, 2001: Numerical simulations of a gravity wave event over CCOPE. Part III: The role of a mountain–plains solenoid in the generation of the second wave episode. *Mon. Wea. Rev.*, **129**, 909–933.
- Kuo, Y.-H., and G. T.-J. Chen, 1990: The Taiwan Area Mesoscale Experiment (TAMEX): An overview. *Bull. Amer. Meteor. Soc.*, **71**, 488–503.
- Kurosaki, Y., and F. Kimura, 2002: Relationship between topography and daytime cloud activity around Tibetan Plateau. *J. Meteor. Soc. Japan*, **80**, 1339–1355.
- Li, Y., and R. B. Smith, 2010: Observation and theory of the diurnal continental thermal tide. *J. Atmos. Sci.*, **67**, 2752–2765.
- Means, L. L., 1954: A study of the mean southerly wind—Maximum in low levels associated with a period of summer precipitation in the Middle West. *Bull. Amer. Meteor. Soc.*, **35**, 166–170.
- Miller, D., and J. M. Fritsch, 1991: Mesoscale convective complexes in the western Pacific region. *Mon. Wea. Rev.*, **119**, 2978–2992.
- Monaghan, A. J., D. L. Rife, J. O. Pinto, C. A. Davis, and J. R. Hannan, 2010: Global precipitation extremes associated with diurnally varying low-level jets. *J. Climate*, **23**, 5065–5084.
- Ninomiya, K., 2000: Large- and meso-a-scale characteristics of Meiyu-Baiu front associated with intense rainfalls in 1–10 July 1991. *J. Meteor. Soc. Japan*, **78**, 141–157.
- Noh, Y., W. G. Cheon, and S. Raasch, 2001: The improvement of the K-profile model for the PBL using LES. Preprints, *Int. Workshop of Next Generation NWP Models*, Seoul, South Korea, Laboratory for Atmospheric Modeling Research, 65–66.
- Pielke, R. A., G. A. Dalu, J. S. Snook, T. J. Lee, and T. G. F. Kittel, 1991: Nonlinear influence of mesoscale land use on weather and climate. *J. Climate*, **4**, 1053–1069.
- Shapiro, M. A., and D. Keyser, 1990: Fronts, jet streams, and the tropopause. *Extratropical Cyclones: The Erik Palmén Memorial Volume*, C. W. Newton and E. O. Holopainen, Eds., Amer. Meteor. Soc., 167–191.
- Shen, Y., A. Xiong, Y. Wang, and P. Xie, 2010: Performance of high-resolution satellite precipitation products over China. *J. Geophys. Res.*, **115**, D02114, doi:10.1029/2009JD012097.
- Skamarock, W. C., J. B. Klemp, J. Dudhia, D. O. Gill, D. M. Barker, W. Wang, and J. G. Powers, 2005: A description of the advanced research WRF version 2. NCAR Tech. Note TN-468+STR, 88 pp.
- Smull, B. F., and R. A. Houze Jr., 1985: A midlatitude squall line with a trailing region of stratiform rain: Radar and satellite observations. *Mon. Wea. Rev.*, **113**, 117–133.
- Sun, J. H., S. X. Zhao, G. K. Xu, and Q. T. Meng, 2010: Study on a mesoscale convective vortex causing heavy rainfall during the Mei-yu season in 2003. *Adv. Atmos. Sci.*, **27** (5), 1193–1209.
- Tao, S. Y., 1980: *Heavy Rainfalls in China* (in Chinese). Science Press, 225 pp.
- Trier, S. B., C. A. Davis, D. A. Ahijevych, M. L. Weisman, and G. H. Bryan, 2006: Mechanisms supporting long-lived episodes of propagating nocturnal convection within a 7-day WRF model simulation. *J. Atmos. Sci.*, **63**, 2437–2461.
- , —, and —, 2010: Environmental controls on the simulated diurnal cycle of warm-season precipitation in the continental United States. *J. Atmos. Sci.*, **67**, 1066–1090.
- Tripoli, G. J., and W. R. Cotton, 1986: An intense, quasi-steady thunderstorm over mountainous terrain. Part IV: Three-dimensional numerical simulation. *J. Atmos. Sci.*, **43**, 894–913.
- , and —, 1989: Numerical study of an observed orogenic mesoscale convective system. Part I: Simulated genesis and comparison with observations. *Mon. Wea. Rev.*, **117**, 273–304.
- Tuttle, J., and C. A. Davis, 2006: Corridors of warm-season precipitation in the central United States. *Mon. Wea. Rev.*, **134**, 2297–2317.
- Wang, C. C., G. T. J. Chen, and R. E. Carbone, 2004: A climatology of warm-season cloud patterns over East Asia based on GMS infrared brightness temperature observations. *Mon. Wea. Rev.*, **132**, 1606–1629.
- , —, and —, 2005: Variability of warm-season cloud episodes over East Asia based on GMS infrared brightness temperature observations. *Mon. Wea. Rev.*, **133**, 1478–1500.
- Wolyn, P. G., and T. B. McKee, 1994: The mountain–plains circulation east of a 2-km-high north–south barrier. *Mon. Wea. Rev.*, **122**, 1490–1508.
- Yu, R., T. Zhou, A. Xiong, Y. Zhu, and J. Li, 2007a: Diurnal variations of summer precipitation over contiguous China. *Geophys. Res. Lett.*, **34**, L01704, doi:10.1029/2006GL028129.
- , Y. Xu, T. Zhou, and J. Li, 2007b: Relation between rainfall duration and diurnal variation in the warm season precipitation over central eastern China. *Geophys. Res. Lett.*, **34**, L13703, doi:10.1029/2007GL030315.
- Zhang, D. L., and J. M. Fritsch, 1988: A numerical investigation of a convectively generated, inertially stable, extratropical warm-core mesovortex over land. Part I: Structure and evolution. *Mon. Wea. Rev.*, **116**, 2660–2687.
- Zhang, F., and S. E. Koch, 2000: Numerical simulation of a gravity wave event observed during CCOPE. Part II: Wave generation by an orographic density current. *Mon. Wea. Rev.*, **128**, 2777–2796.
- Zhang, S. L., S. Y. Tao, and Q. Y. Zhang, 2002: Large and mesoscale characteristics of intense rainfall in the mid and lower reaches of the Yangtze River. *Chin. Sci. Bull.*, **47** (9), 779–786.
- Zhang, X. L., S. Y. Tao, and S. L. Zhang, 2004: Three types of heavy rainstorms associated with Mei-yu front (in Chinese). *Chin. J. Atmos. Sci.*, **28** (2), 187–205.
- Zhao, S. X., Z. Y. Tao, J. H. Sun, and N. F. Bei, 2004: *Study on Mechanism of Formation and Development of Heavy Rainfalls on Mei-Yu Front in Yangtze River* (in Chinese). China Meteorological Press, 282 pp.